Materials Research.
DOI: http://dx.doi.org/10.1590/1980-5373-MR-2018-0038

Effect of Flame Spray Deposition Parameters on The Microstructure of Al_2O_3 - 13 %TiO_2 Coatings Applied Onto 7075 Aluminum Alloy

José Alexander Arboleda[a]*, Carlos Mario Serna[a], Edwin Cadavid[b], Augusto Cesar Barrios[a], Fabio Vargas[b], Alejandro Toro[a]

[a]*Grupo de Investigación en Tribología y Superficies, Universidad Nacional de Colombia, Medellín, Colombia*
[b]*Grupo de Investigación de Pirometalurgia y Materiales, Universidad de Antioquia, Antioquia, Medellin, Colombia*

Received: January 12, 2018; Revised: March 30, 2018; Accepted: May 20, 2018

In this work, the effect of flame spraying parameters on physical, structural and microstructural characteristics of Al_2O_3 - 13 wt.% TiO_2 (AT-13) coatings were studied. NiCrAl and AT-13 feedstock powders were used for spraying a bond coat (BC) and a top coat (TC), respectively, onto a 7075 aluminum alloy substrate. The effect of acetylene-to-oxygen ratio and the spraying distance on surface roughness, crystalline phases, porosity and thickness of top coat were analyzed. The results showed that for the evaluated spraying conditions, the volumetric oxy-fuel ratio had significant effects on roughness, porosity and crystalline phases of the coating. On the other hand, the spraying distance affected the thickness of the coating and did not influence the formation of Al_2TiO_5 phase; no significant effect of spraying distance on roughness was observed. The results showed that an acetylene: oxygen volumetric ratio of 1:2.5 is preferable to obtain higher melting of the ceramic powders and therefore a denser coating with major content of γ-Al_2O_3 crystalline phase.

Keywords: *Flame spraying, crystalline phase, amorphous phase, porosity, roughness, design of experiment.*

1 Introduction

The competitiveness of ceramic coatings has evolved over the years thanks to developments in thermal spraying coatings, processes and devices used for this purpose, as well as the increase in the number and variety of applications including thermal protection of components located in the hot gas path of gas turbines, improvement of wear resistance of automotive engine devices and medical implants, among others[1]. Regarding thermal spraying processes, flame spraying is the oldest and most used in industrial applications [2]. However, the development of new applications for ceramic coatings manufactured by Atmospheric Plasma Spraying (APS) has increased notably in recent years due to the higher temperature and speed of the particles achieved in this process, which allows manufacturing denser and most adhesive coatings[3]. Consequently, a reduction in the number of investigations carried out to develop new coatings and to improve the performance of coatings deposited by flame spraying is evident despite its lower operation cost, ease of use and flexibility for selecting a range of flame temperature profiles from the combustible/comburent ratio[4] ; all these, depending on the feedstock materials and feed rates.

Aluminum alloys are preferred as structural components due to their high strength-to-weight ratio. However, they have low wear resistance which limits their use[5]. Alloys such as the 7075-T6 are widely used for aeronautic applications, but depending of the environmental conditions, this material may suffer several types of corrosion damage. Consequently, surface protection of 7075-T6 alloy with the aid of thermal spraying processes has been increasingly studied, being Ti, Al_2O_3, ZrO_2 and TiO_2 some of the materials commonly chosen to provide protection against corrosion and wear[5,6].

The thermally-sprayed AT-13 coatings are widely used in tribological applications given the variety of mechanical properties that can be obtained as a function of the stable and metastable phases present in the microstructure and the morphological features of the coatings[7]. Typical phases found in AT-coatings include α-Al_2O_3, γ-Al_2O_3, TiO_2 and Al_2TiO_5[8] . Aluminum titanate (Al_2TiO_5) is desirable for applications involving high temperature due to its low thermal expansion coefficient ($1.5x10^{-6}$ K^{-1}), low thermal conductivity (0.9-1.5 Wm^{-1} K^{-1}), low Young's modulus (10-20 GPa) and high melting point (1860 ± 10ºC)[9,10]. Additionally, Al_2TiO_5 has been used by the industry because it has high thermal shock and corrosion resistances[10]. Rutile (TiO_2) also exhibits good corrosion resistance combined with excellent chemical stability in aqueous environments[11] while α-Al_2O_3 is a good choice for wear and corrosion aplications due to its high hardness and chemical inertness[12]. For use in thermal spraying processes, the stability of aluminum titanates is improved by adding modifying agents such as SiO_2, MgO and Fe_2O_3 to the powder[13], which hinders the decomposition of the phase at high temperature. Currently, highly improved AT-13 coatings are being manufactured from

*e-mail: jaarboledag@unal.edu.co

nanoagglomerated feedstock powders in order to obtain a bimodal structure constituted by fully and partially melted splats, which notably improve the mechanical and tribological properties of the coating as reported by [14] and[15].

Phase contents and porosity are determinant for the wear and corrosion resistances of AT-13 coatings as previously stated by Aruna et al[1], Ibrahim[16] and Yussoff et al [17], among others. Accordingly, establishing proper thermal spray deposition conditions is key to prevent premature failure of the coatings, which are commonly used to protect surfaces against elevated temperature and/or harsh environments. This work studied the effect of the spraying distance and the oxygen:acetylene volumetric ratio on the microstructure of coatings composed of NiCrAlY as Bond Coat (BC) and Al_2O_3 - 13%wt. TiO_2 as Top Coat (TC), with the purpose of improving the combined response of the surface to mechanical, thermal and chemical requirements. The characterization of the coatings included crystalline phase identification and quantification, surface texture assessment and detailed analysis of morphological features such as unmelted particles, splats/lamellae, pores and cracks.

2 Experimental Procedure

2.1 Powders characterization

The particle size distribution of feedstock powders Metco 6221 (Al_2O_3 - 13 wt. % TiO_2) and Amdry 510 (NiCrAlY) was determined using a Malvern Master Sizer 2000 analyzer. Morphological characterization of feedstock powders was made in a JEOL 6701 SEM. Additionally, the identification of the crystalline phases was carried out by X-Ray diffraction (XRD) using a PANAlytical Empyrean III series Alpha 1 model 2012 diffractometer with CuKα radiation and X'Pert Pro MDPsoftware.

2.2 Flame spraying process

Prior to the spraying process, the AA7075 substrates were cleaned in ultrasonic bath with isopropyl alcohol then the surface was corundum blasted and finally cleaned again in the ultrasonic bath with isopropyl alcohol for removing impurities. This procedure allowed obtaining surfaces with Ra = 6.33 ± 0.84 µm, Rt = 53.86 ± 10.10 µm and Rpc = 72. 42 ± 8.84 cm^{-1}.

The bond and top coatings were deposited with a Castolin-Eutectic TeroDyn® 2000 system torch, in which the powders were fed using a bowl feeder TUMAC CHTB-10 and nitrogen as carrier gas. The preheating temperature of substrates was measured using a RayTek MI infrared sensor. The spraying parameters controlled during thermal spraying processes carried out to manufacture the coatings are listed in Table 1.

In order to study the effect of standoff distance and acetylene:oxygen volumetric ratio on roughness, porosity, thickness, and formation of crystalline phases in the AT-13 top coatings, the spraying distance (110 and 140 mm), and the acetylene:oxygen volumetric ratios (1:1.7 and 1:2.5) were selected according to a factorial design of experiments 2^2 with three replicas per spraying condition and a central point at 125 mm of spraying distance and a flame gases ratio at 1:2.1, as shown in Table 2. A confidence level of 98% was taken for the statistical evaluation of the experiments. Thirteen experimental runs were executed randomly to verify the repeatability of the experiment and the uniform distribution of experimental error. The *p*-value was also considered to evaluate the significance of the effects on roughness and phases formation. Porosity and thickness of the coating were also studied by means of effects plots to estimate the tendencies of those characteristics in the coatings.

Table 1. Spraying parameters used to manufacture the coatings

Parameter	Operation value	
	Bond Coat	Top Coat
Standoff distance (mm)	150	110-140
Substrate rotational speed (rpm)	116	
Translational speed of the torch (cm/s)	0.72	
Preheating passes	1	
Spraying passes	4	5
Acetylene flow (L/min)	22	24
Oxygen flow (L/min)	37	41-60
Acetylene pressure (psi)	12	
Oxygen pressure (psi)	50	
Powder feed rate (g/min)	25	13
Nitrogen carrier gas flow (L/min)	17	
Nitrogen carrier gas pressure (psi)	40	

Table 2. Spraying parameters used to manufacture the Top Coats according to the factorial Design of Experiments.

Coating code	Spraying parameters		
	Combustion ratio (C_2H_2:O_2)	Standoff distance (mm)	Pre-heat temperature (ºC)
S1	1:1.7	110	98
S2	1:1.7	140	78
S3	1:2.5	110	96
S4	1:2.5	140	78
Central Point	1:2.1	125	85

1:1.7 -» 24:40.8 (L/min) 1:2.5 -» 24:60 (L/min)

2.3 Coatings characterization

Surface roughness of the BC and TC layers was determined using a Mitutoyo Surftest SV-3000; six profiles of each sample were obtained. The measurements

were made with five cut-off lengths of 2.5 mm for a total sampling length of 12.5 mm. The surface roughness parameters Ra, Rt, RSM, Rpc and power spectral density (PSD), whose definition can be found elsewhere[18], were measured after all experiments.

X-ray diffraction of the coatings were carried out using an X'Pert Pro MPD. The diffractograms of the coatings manufactured according to each spraying condition were compared to confirm the repeatability of the experiments. Crystalline phases present in the coatings were quantified by Rietveld refinement using MAUD (*Materials Analysis Using Diffraction*) software, always verifying that Rwp < 10%. A seventh degree polynomial was used to model the background noise of the diffractograms while scale factor, crystal structure, parameters for texture, strain analysis, among other parameters, were refined using from 9 to 12 iterations for each one. Amorphous phase content was also computed through Le Bail approximation for the silica glass. The Rietveld method approximates the amorphous phase to a nanocrystalline solid where the long-range order is lost[19] and the Le Bail approximation has been used to analyze the semi-crystalline pattern of several ceramics including α-Al_2O_3[20].

Structural characterization of the coatings were performed using SEM Jeol 5910LV. The cross section of the coatings was also analyzed from samples prepared according to ASTM E 1920-03(2014) standard; porosity of the BC and TC was measured in the cross section using digital image processing according to the ASTM E2109-01 standard. For the BC, oxides were quantified using the red histogram in the color thresholding process in order to exclude them of readings carried out to measure the porosity. The thickness of the coatings was measured through optical microscopy.

3 Results and Discussion

3.1 Feedstock powders

The Amdry 510 and Metco 6221 powders showed spheroidal morphology. Amdry 510 is compact as those produced by gas atomization, which is a process widely used to manufacture metal alloy powders[21]. In the Metco 6221, each particle is constituted by several agglomerated submicron-particles, which is consistent with manufacturing by agglomeration and sintering. The particle size distribution of the powders is shown in Table 3.

Table 3. Particle size distribution of Amdry 510 and Metco 6221 powders.

Powder	d(0.1) µm	d(0.5) µm	d(0.9) µm
Amdry 510	26.994	36.893	50.151
Metco 6221	25.433	34.989	48.405

The phases identified in feedstock powders and their quantities are summarized in Table 4. γ-Ni,Cr, γ'-Ni_3Al and β-AlNi were found in Amdry 510 powder while α-Al_2O_3, Al_2TiO_5 and low quantities of TiO_2-rutile were identified in Metco 6221 powder after XRD analyses. Metallic alloys containing the phases identified in Amdry 510 powder are normally used to apply the bond coat in components for stationary and aircraft gas turbines thanks to their high mechanical resistance despite their lower resistance to sulfidation when compared to the CoCrAlY bond coatings [22]. On the other hand, α-Al_2O_3-13 wt.% TiO_2 materials with phases as those constituting Metco 6221 powder provides good tribological properties due to their high hardness, which help withstanding severe abrasive wear conditions[23].

Table 4. Phase analysis of feedstock powders

Powder	Phase analyses		Weighted R Profile %
	Phase	Wt. %	
Amdry 510	Ni,Cr (γ)	44.2	9.98
	Ni_3Al (γ)	28.4	
	AlNi (β)	27.5	
Metco 6221	α-Al_2O_3	73	5.86
	Al_2TiO_5	22.7	
	TiO_2-rutile	4.3	

3.2 Bond coat characterization

The XRD results of NiCrAlY coating and powders are shown in Figure 1. Rietveld analysis of as-sprayed BC with an Rwp of 6.54% showed 99.7% of phase γ'-Ni_3Al and only 0.3% of β-AlNi. No γ phase was identified in the as-sprayed

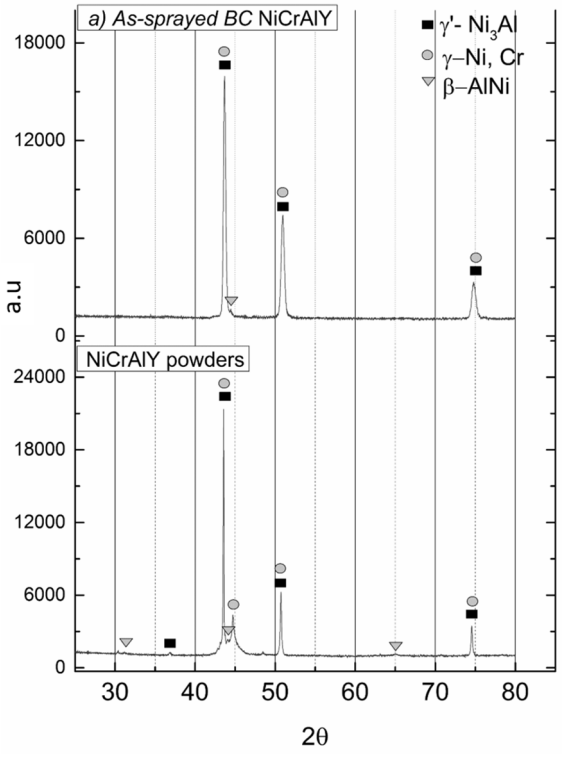

Figure 1. XRD of NiCrAlY coating. a) As-sprayed BC, b) Feedstock powder

BC as reported previously by[24]. A slight peak shift was also observed, which can be related to quenching stresses produced when the particles reached the substrate and rapidly solidified. In flame spraying process, unlike HVOF process, aluminum gets oxidized extensively forming Al_2O_3 during deposition, contributing also to the peaks shift as reported by Rana et al[24].

The surface morphology of the bond coat exhibited splats produced from highly flattened particles and splashing as shown in Figure 2a (yellow enclosure), which indicates that in-flight particles were sufficiently heated and arrived well melted to the surface on which they were deposited. Despite the diffractograms did not show strong evidences of oxides likes Al_2O_3, the BC layer showed oxides content of 18 ± 1.90% and porosity of 6.73 ± 0.98%. Likewise, the cross-section of the BC layer Figure 2b exhibited oxidized areas around lamellae which were produced during the spraying process due to the slightly oxidizing combustion flame used for the deposition of this layer. The oxidation of some elements present in the thermally sprayed metallic powder NiCrAlY are reported by Rana et al [24,25] where alumina is the oxide predominantly produced, which increases the oxidation resistance of the coating. The arithmetic average roughness Ra of the bond coat was 9.4 ± 1.8 µm.

3.3 Top coat characterization

3.3.1 Analysis of crystalline phases in the microstructure

The X-Ray diffractograms of the AT-13 coatings obtained with different deposition parameters are shown in Figure 3. For each spraying condition, the diffractograms of the three replicas are superimposed. The AT-13 coatings S3 and S4 (figures 3a and 3b) were composed of cubic γ-Al_2O_3 and rhombohedral α-Al_2O_3. The coatings S1 and S2 (Figure 3c and Figure 3d) showed γ-Al_2O_3, α-Al_2O_3 and orthorhombic Al_2TiO_5. TiO_2-rutile, which was present in feedstock powder, was not found in any of the deposited coatings.

The assumptions of normality and constant variance of the phase contents data were verified through the normal probability and residuals plots. To check for the normality of the residuals (i.e. the fact that residuals follow a normal distribution), the normal probability plot is presented in figure 4a with the data obtained for γ-Al_2O_3. Residuals follow a straight line, which is a strong indication that the assumption of its normality is valid. Furthermore, the plot of residuals vs fitted values Figure 4b shows a random scattering of residuals around zero, which verifies the assumption of constant variance of the experiments. These facts were also observed in the evaluation of the assumptions of normality and constant variance for the other crystalline and amorphous phases found in the samples.

Quantitative phases analysis of the coatings evidenced a higher content of γ-Al_2O_3 in coatings S3 and S4, while S1 and S2 coatings were constituted predominantly by α-Al_2O_3 and some quantities of Al_2TiO_5 which are residual phases that were present in feedstock powders. Coatings S3 and S4 sprayed with a combustion ratio of 1:2.5 showed amorphous content of 47.20% and 42.35% respectively, while the amorphous content of coatings S1 and S2 were 12.26% and 10.58% respectively (Figure 5d). These results show that when the particles absorb more energy in the flame, higher amorphous phases are obtained. However, the amorphous percentage estimated can be affected also by the presence of γ-Al_2O_3 which is a nanosized crystalline phase[26], whose volume fraction is higher in coatings S3 and S4.

The plots of the effects of spraying parameters vs phases present in the coatings are shown in Figure 5. A *p*-value < 0.02 was obtained for the effect of the combustion ratio on the α-Al_2O_3 phase content in the coatings. It means that this parameter had an important effect in α-Al_2O_3 phase transformation during the spraying process. Regarding the effect of spraying distance on α-Al_2O_3 transformation, the *p*-value was 0.485; this means that this parameter did not have a significant impact on the α-Al_2O_3 transformation;

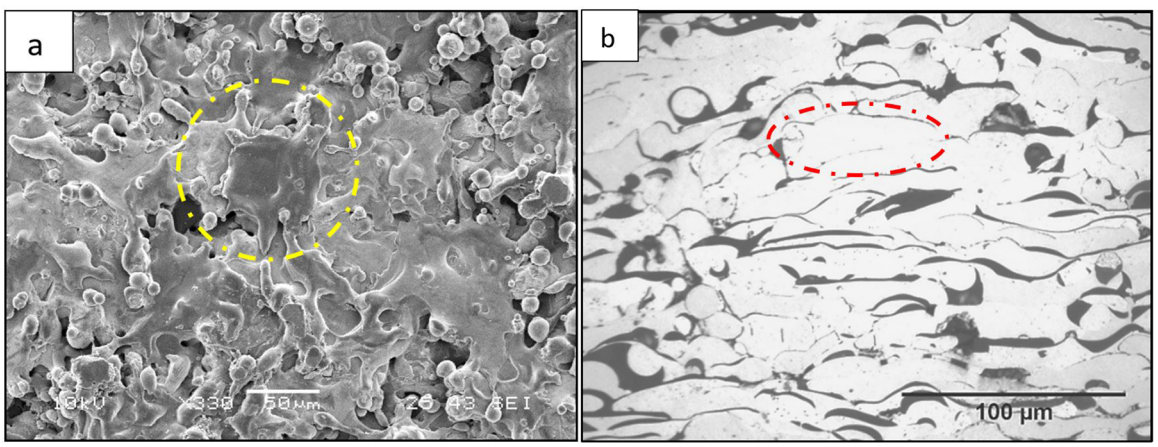

Figure 2. Microstructure of the Bond Coat. a) surface morphology in which an individual splat is shown within the yellow circle, b) cross section morphology in which an individual lamella is shown within the red oval

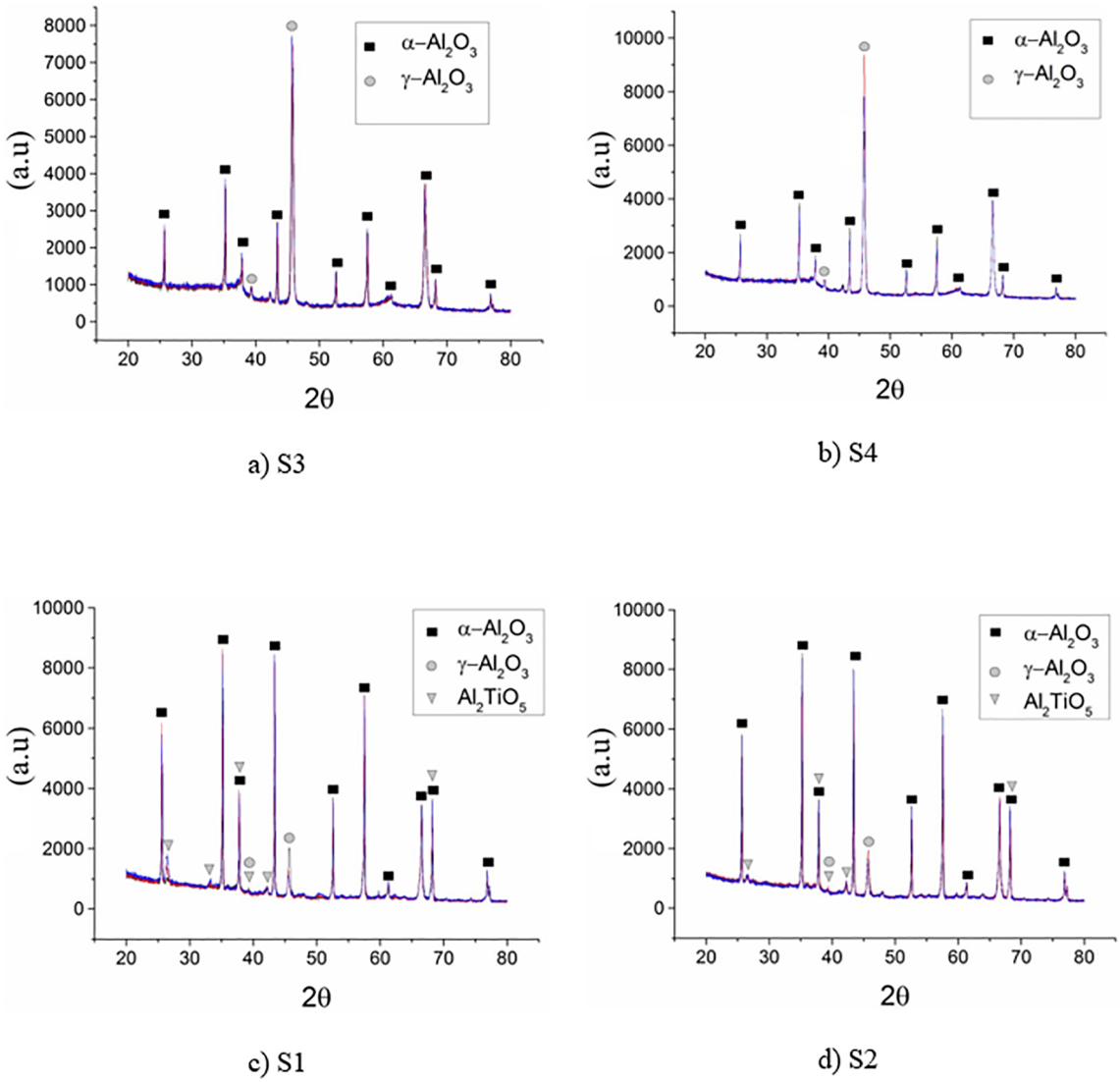

Figure 3. X-Ray diffractograms of AT-13 coatings for several oxygen: acetylene volumetric ratios and spraying distances. a) Coating S3: 1:2.5 - 110 mm, b) Coating S4: 1:2.5 - 140 mm, c) Coating S1: 1:1.7 - 110 mm, d) Coating S2:1:1.7 - 140 mm

to show graphically this result, it can be seen in figure 5a that for a fixed combustion gases ratio, variations on spraying distance did not produce significant changes on the α-Al_2O_3 phase transformation. For example, with a fixed combustion ratio 1:1.7, an increase of the spraying distance from 110 mm to 140 mm only produces a decrease of 5% in the mean content of α-Al_2O_3. It is important to note also in Figure 5a that the deviation bars of α-Al_2O_3 content in both combustion ratio are overlapping for changes in spraying distance, this is the main graphically aspect that evidence why this parameter did not have a significant effect on this phase.

For the combined effect of the spraying distance and combustion ratio on α-Al_2O_3 transformation, the *p*-value was 0.545; this means that it did not have a significant impact on this phase transformation. The combined effect indicates that when a variation of combustion ratio is made there is a relevant change in the amount of α-Al_2O_3 with variations of spraying distance, same logic is applicated with the other phases analyzed. Figure 5 a shows that it does not matter the combustion ratio set, for both, 1:1.7 and 1:2.5, changes in spraying distance did not produce important variation in the α-Al_2O_3 phase content.

Figure 5b shows that the coating deposited with a combustion gases ratio 1:2.5 exhibited a major formation of γ-Al_2O_3 as a consequence of the transformation of α-Al_2O_3 from the feedstock powders during the solidification at high cooling rates of the splats, as explained in detail by Góral et al[27] and Vargas et al[28]. This is consistent with the reduction of α-Al_2O_3 phase content observed in figure 5a for the same combustion ratio.

With respect to the γ-Al_2O_3 formation, a *p*-value < 0.02 for the effects of the combustion gases ratio was obtained while

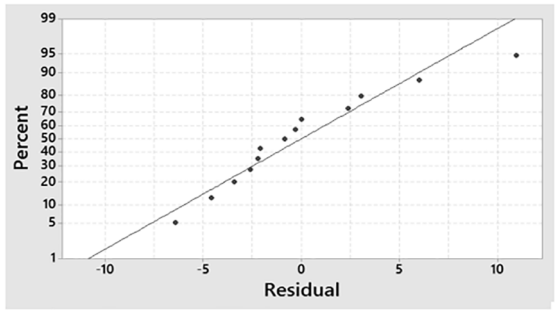

a)

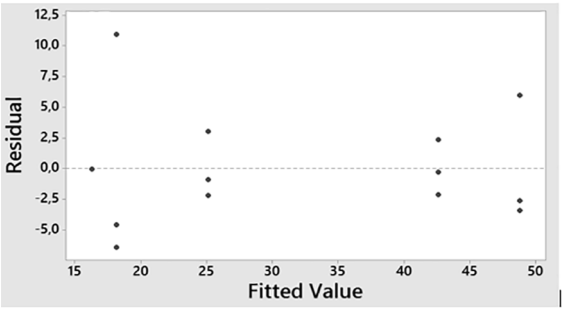

b)

Figure 4. Residual plots for γ-Al_2O_3. a) normal probability plot, b) residual vs fitted values

the spraying distance yielded a *p*-value = 0.080. This means that the combustion gases ratio had a significant effect on the γ-Al_2O_3 formation and the spraying distance did not had effect on the formation of this phase; besides, for the combined effect of spraying parameters evaluated, a *p*-value=0.911 evidencing that for both combustion ratios, variations in spraying distances did not have a significant effect on the formation of γ-Al_2O_3.

The increase in γ-Al_2O_3 at ratio 1:2.5 was affected also by Al_2TiO_5 thermal instability in a range of temperatures between 800 and 1300°C where an eutectoid reaction occurs and decomposes it into α-Al_2O_3 and TiO_2 as suggested by Papitha et al[9] and Sarkar et al[10]; During the spraying process, α-Al_2O_3 and TiO_2 melt together and rapidly solidify to form γ-Al_2O_3 containing dissolved TiO_2[26]. This can be verified in Figure 5c, where for a fixed distance, the Al_2TiO_5 content is lower at combustion gases ratio 1:2.5 with respect to 1:1.7. The eutectoid reaction of Al_2TiO_5 was facilitated because the particles had a higher dwelling time inside the flame during the spraying process, allowing them to absorb a higher energy to reach the temperatures of decomposition. For the Al_2TiO_5, *p*-value<0.02 was obtained for the effect of the combustion gases ratio meaning that it had a significant effect on the eutectoid reaction of this phase during the

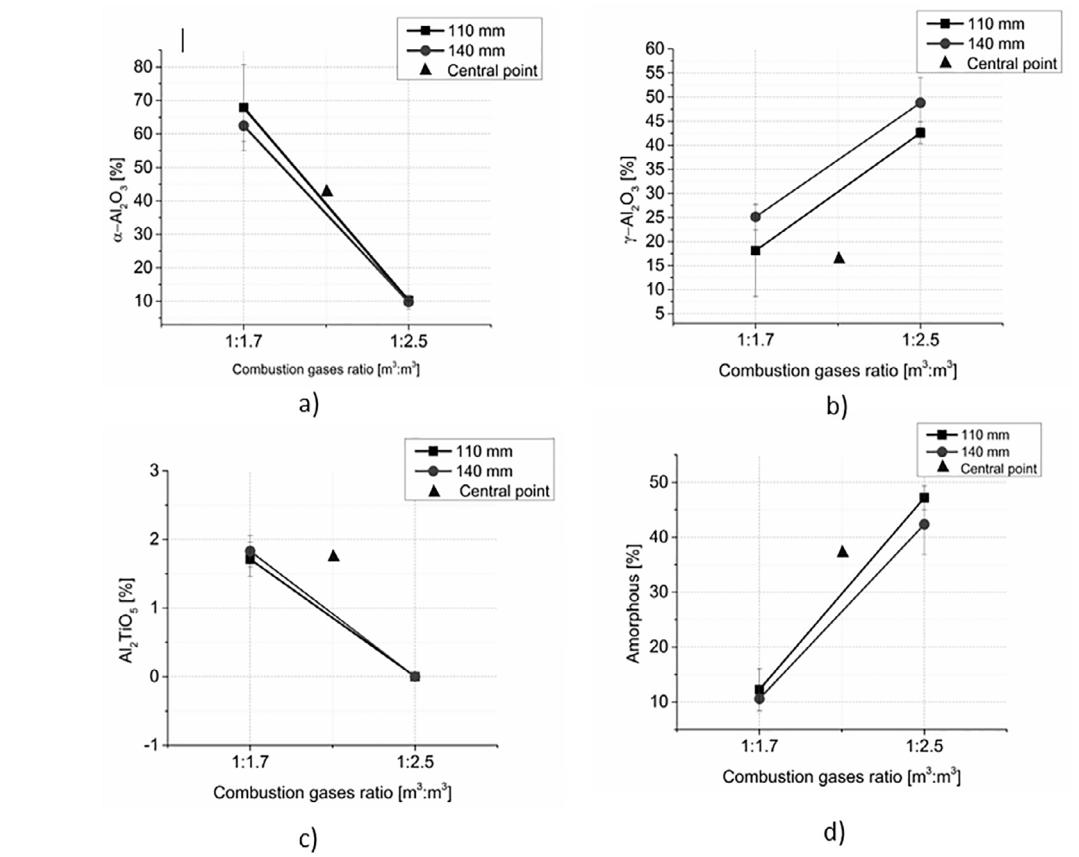

Figure 5. Effect of Combustion gases ratio and spraying distance on phases formation, a) α-Al_2O_3, b) γ-Al_2O_3, c) Al_2TiO_5, d) Amorphous phase

spraying process; on the other hand, a *p*-value = 0.573 was obtained for both the spraying distance and its combined effect with combustion gases ratio, so it can be said that no important effect of such variables on the decomposition of this phase is expected.

With respect to the amorphous content in the coating, a *p*-value < 0.02 obtained for the effect of combustion on this phase indicated that it had an important effect on this variable response, while the spraying distance did not affect it according to the *p*-value=0.163 obtained. The combined effect of spraying distance and combustion ratio did not have significand impact on the amorphous content as indicated by a *p*-value of 0.478.

Curvature analysis of the effect of spraying parameters on phase formation shows *p*-value of 0.392 and 0.019 for α-Al_2O_3 and γ-Al_2O_3 respectively, revealing that there is not curvature in the response of α-Al_2O_3, and a marginal curvature in the response for γ-Al_2O_3 phase; on the other hand, *p*-value for curvature of Al_2TiO_5 was 0.001, this suggests that there is curvature in the response of this phase with respect to the spraying parameters inside the experimental region evaluated.

3.3.2 Roughness, morphology and porosity of the coatings

Normal probability plot and residuals vs fitted plots for the Rms roughness parameter are shown in Figure 6. It can be seen from Figure 6a that residuals follow a straight line while Figure 6b shows a random scattering of residuals about zero. This means that there is no evidence of non-normality and non-constant variance in the experiments; these facts were also observed for the other roughness parameters evaluated.

Roughness parameters of the TC are shown in the effects plots of flame spraying parameters onto surface roughness (Figure 7). A *p*-value = 0.008 (<0.02) for the effect of the combustion gases ratio on the surface roughness was obtained, while the *p*-values of spraying distance and the combined effect of the spraying distance and combustion gases ratio were 0.386 and 0.964 respectively (both >0.02). This means that only combustion gases ratio had a significant effect on the coatings surface roughness. On the other hand, curvature analysis shows *p*-values of 0.199, 0.030, 0.021 and 0.678 for RSm, Ra, Rt, and Rpc parameters respectively, this mean that there was not curvature in the response of the roughness parameters studied. Higher roughness values were obtained with a combustion gases ratio of 1:1.7, and this is because the coatings S1 and S2 had a higher number of unmelted particles than that of the coatings S3 and S4 sprayed with combustion gases ratio of 1:2.5 as verified by means of SEM analysis whose results are shown in Figure 8. Figure 7 also shows that with a fixed combustion gases ratio, variations of spraying distance had not a considerable impact onto surface roughness; On the other hand, when the spraying distance was fixed, variations of combustion gases ratio had a high impact onto surface roughness. According

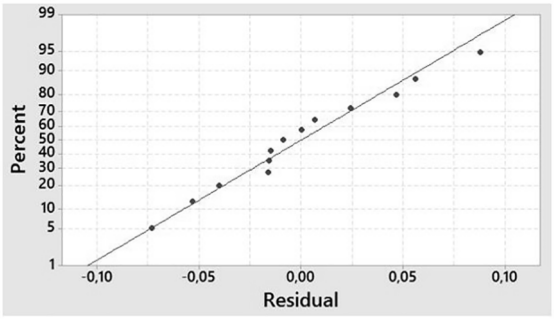

a)

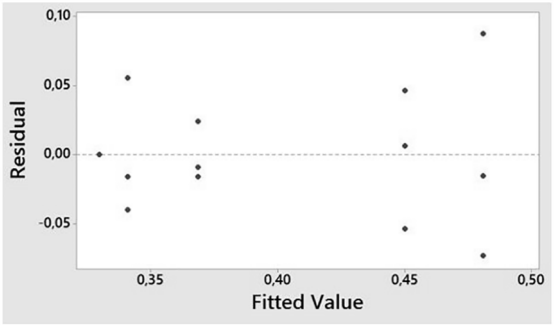

b)

Figure 6. Residual plots for RSM roughness parameter. a) normal probability plot, b) residual vs fitted plot

to the measured roughness parameters, a smoother surface can be obtained with the combustion gases ratio used for manufacturing S3 and S4 coatings. Figure 8 shows that effectively, coatings S3 and S4 presented a lower number of unmelted and partially-melted particles on their surfaces, this means that the AT-13 particles reached higher temperatures with a combustion gases ratio of 1:2.5 in their flying time during the spraying process.

Figure 9 shows the cross section of the applied coatings. The coatings sprayed with combustion ratio 1:2.5 (Figures 9a and 9b) present a denser microstructure because the particles reach higher temperatures and consequently experience more softening and deformation when they strike the substrate's surface. This leads to the formation of flatter lamellae in comparison with the coatings sprayed with combustion ratio 1:1.7, whose cross section shows a larger porosity due to the presence of a greater number of unmelted and partially melted particles (figures 9c and 9d). Furthermore, microstructure defects such as pores and cracks reduce the bonding strength between splats, which in turn affects other properties including hardness and abrasion resistance[29].

The size of unmelted and partially-molten particles was measured through SEM and the data were used to perform spectral analysis as shown in Figure 10 and Table 5. The increase of the minimum and maximum diameters of semi-molten particles with respect to d(0.1) and d(0.9) of feedstock powders was due to the deformation of the particles during

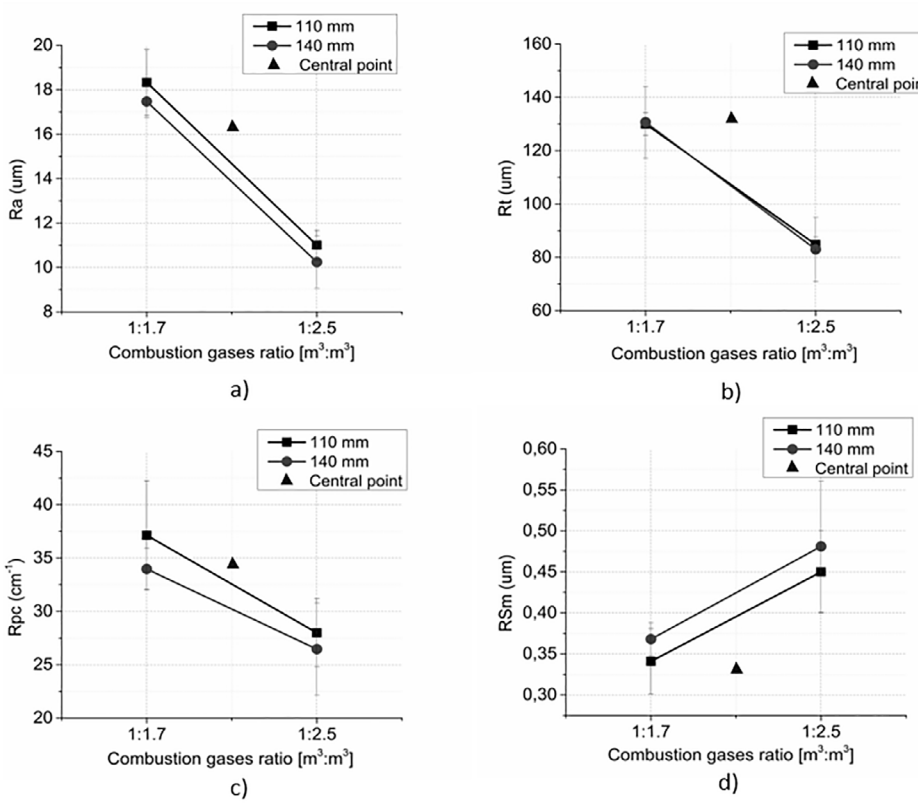

Figure 7. Effect of spraying parameters on roughness parameters a) Ra, b) Rt, c) Rpc, d) RSM

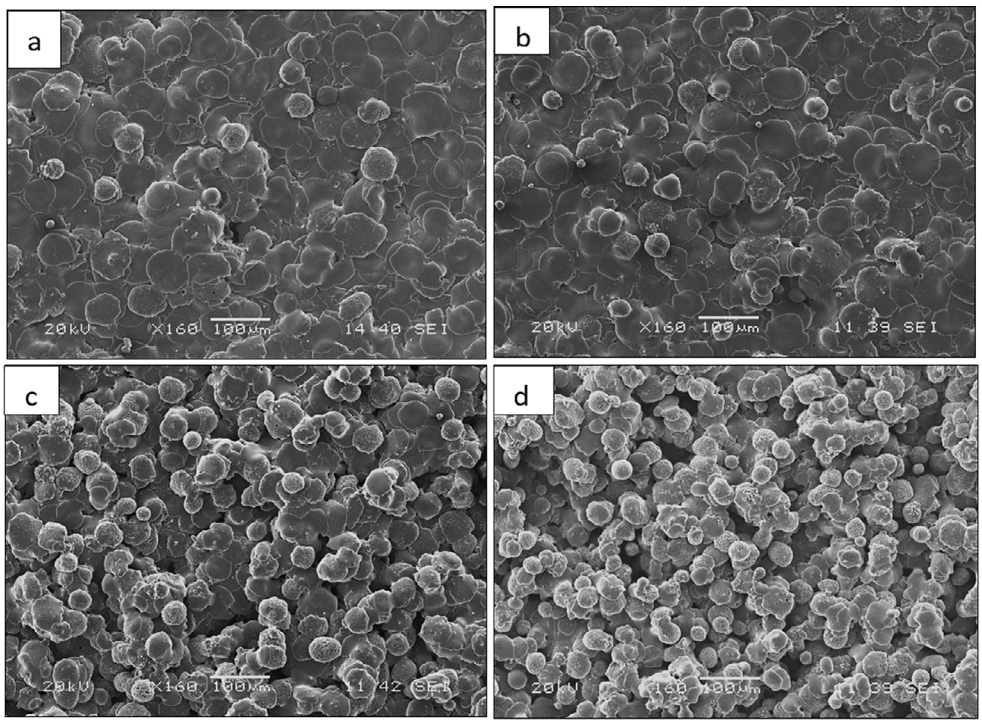

Figure 8. AT-13 coatings surface morphology. a) 1:2.5 - 110 mm, b) 1:2.5 - 140 mm, c) 1:1.7 - 110 mm, d) 1:1.7 - 140 mm

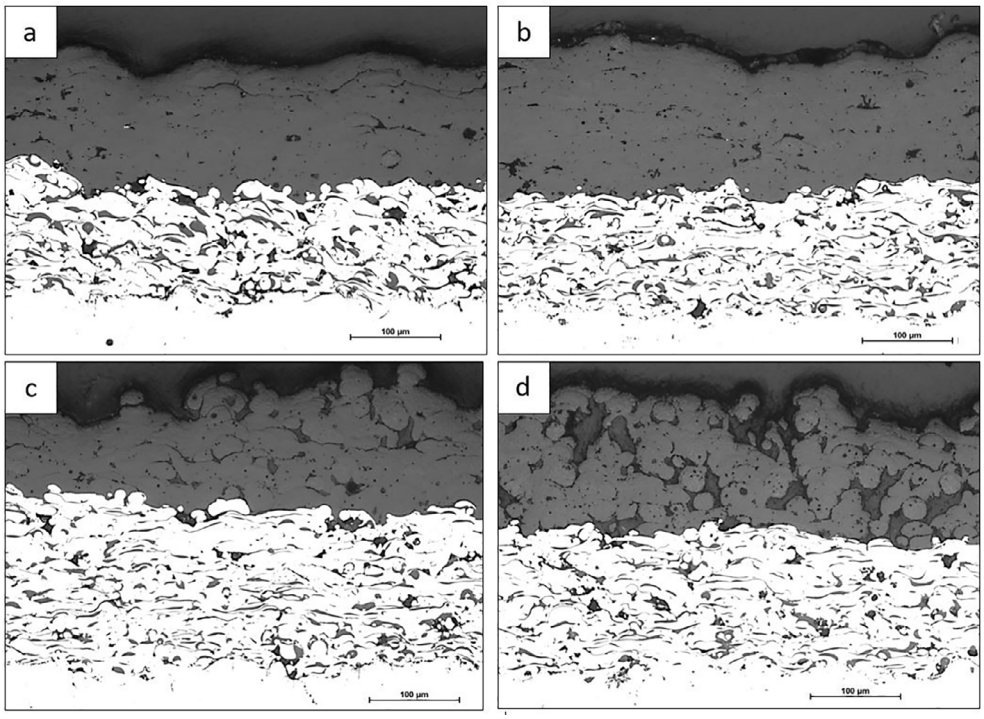

Figure 9. Aspect of the cross section of AT-13 coatings deposited with diverse oxygen: acetylene volumetric ratios and spraying distances. a) 1:2.5 - 110 mm, b) 1:2.5 - 140 mm, c) 1:1.7 - 110 mm, d) 1:1.7 - 140 mm

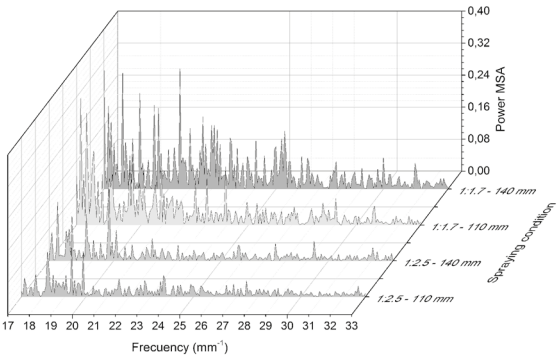

Figure 10. Power Spectral Density (PSD) of AT-13 coatings surfaces

the impact against the substrate. On the other hand, the minimum diameter of unmelted particles measured in the surface coating was 30.44 µm, which means that the heat produced in the flame is enough to melt particles smaller than approximately 30 µm. The Power Spectral Density (PSD) plot in Figure 9 shows a higher intensity in the frequency range from 17 to 23 mm^{-1} for the coatings sprayed with a combustion gases ratio of 1:1.7; this verifies that a higher quantity of semi-molten particles with sizes between 43 and 59 µm can be found along the roughness profile measured in the S1 and S2 coatings with respect to S3 and S4 coatings. In the frequency range between 25 and 33 mm^{-1} the intensity was lower in the spectra corresponding to coatings sprayed with combustion gases ratio of 1:2.5, which indicates that these coatings have a lower quantity of unmelted particles with sizes between 30 and 45 µm.

The effect of the spraying parameters on the thickness of the TC layer is shown in Figure 11. An important effect of the spraying distance on the thickness of the coating can be appreciated. The use of a spraying distance of 110 mm led to thinner coatings when compared to the coatings sprayed with 140 mm distance, this is due to higher deceleration and slight cooling of the particles in the latter case, which in turn causes less deformation of the particles when they impact the substrate. Consequently, slower particles produce thicker lamellae and the overall thickness of the coating is larger. Figure 9 illustrates this effect. Figures 9 and 9d show thicker lamellae than those observed in figures 9a and 9c. It can be seen also that with a fixed spraying distance, variations in the combustion gases ratio did not contribute strongly to changes in the thickness of the coatings.

The effect of the spraying parameters on the porosity of the coatings is reported in Figure 12. Coatings S3 and S4 had lower porosity values than S1 and S2 coatings and close to the values reported by[30] for an AT-13 coating deposited by APS, which is a process with higher enthalpy. Figure 11 shows that variations in spraying distance when the combustion gases ratio is fixed at 1:2.5 did not have and important effect on the porosity of the coatings; however, with a combustion gases ratio fixed at 1:1.7, distance variation affects the coatings porosity incrementing it in the coatings deposited with a spraying distance of 140 mm. This may

Table 5. Attributes of interest after PSD analysis.

Attribute	Minimum diameter (μm)	Spatial Frequency (mm^{-1})	Maximum diameter (μm)	Spatial frequency (mm^{-1})
Semi-molten particles	42.74	22.39	56.46	17.71
Unmelted particles	30.44	32.85	45	21.37

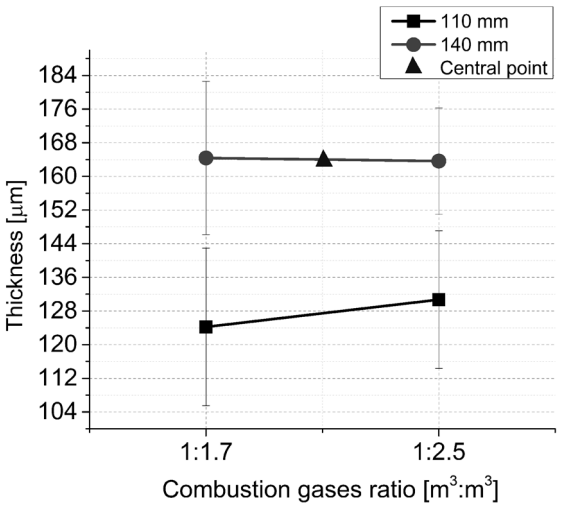

Figure 11. Effects plot of spraying parameters on coating thickness

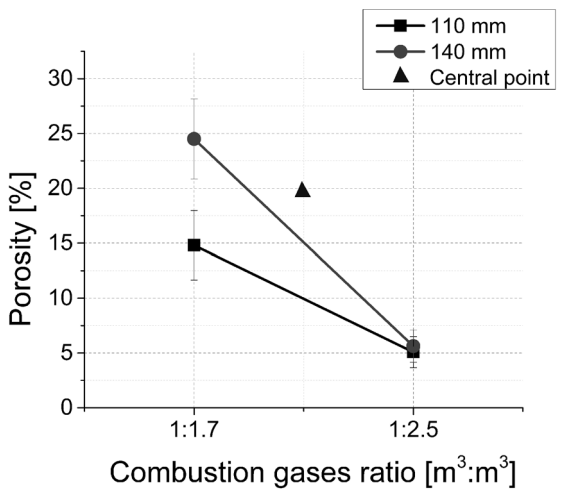

Figure 12. Effects plot of spraying parameters on coatings porosity

also be related to the higher deceleration of the particles with the distance, which leads to poor piling and adhesion between particles in the coating.

3.3.3 Analysis of the quality of the flame

In general terms, it was observed that S3 and S4 coatings exhibited lower values of the roughness parameters and porosity; XRD analysis also showed highest formation of γ-Al_2O_3 and also highest decomposition of Al_2TiO_5 for those coatings. These results indicated that particles absorbed more heat during the spraying process at the flame produced from combustion gases ratio of 1:2.5, than that produced from 1:1.7 combustion gases ratio; despite the higher temperature of flame from 1:2.5 combustion gases ratio is lower than that produced from 1:1.7 combustion gases as demonstrated by Fauchais et al [2].

Besides the temperature reached by the flame, which is shown in figure 13 for several oxy/acetylene ratios, the length of the hot zone of the flame obtained with different comburent/combustible ratios must be considered since it plays a key role in the heating of the particles. At atmospheric pressure, the stoichiometric chemical reaction of combustion is obtained by feeding the torch with a volumetric mixture of acetylene and oxygen in proportions around 1:1.7, producing a flame whose primary zone reaches the maximum possible temperature, which is close to 3170 ºC. When an additional quantity of oxygen is fed to the torch, part of the heat produced by the combustion is consumed in heating up the excess gas because it does not react in the process, then the temperature of flame decreases as it has been shown by Fauchais et al[2]. Also, Góral showed that the excess of oxygen in a combustion reaction contribute to dilute the combustion products and causes elongation of the primary zone of the flame and therefore a change of his temperature profile, providing the particles a longer dwelling time in the hottest zone of the flame when combustion gases ratio is 1:2.5 compared to when the combustion gases ratio is 1:1.7 [31].

4 Conclusions

The effect of the volumetric combustion gases ratio and spraying distance on structural and microstructural characteristics

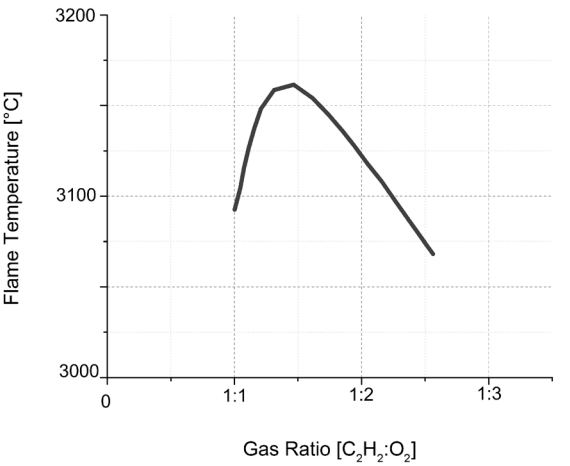

Figure 13. Temperature profile for oxy-acetylene combustion (2)

of the Al_2O_3 - 13 wt.%TiO_2 coatings manufactured by flame spraying process was studied.

The most significant effect over the formation of γ-Al_2O_3 crystalline phase was given by the combustion gases ratio. Higher levels of crystalline phase formation were achieved when the combustion gases ratio was 1:2.5, which is due to the elongation of the hottest zone of the oxyacetylene flame produced by the excess of oxygen in the combustion reaction. On the other hand, Only combustion gases ratio had a significant effect on α-Al_2O_3 formation and Al_2TiO_5 dissolution.

Only the combustion gases ratio had a significant effect on the roughness parameters of the coating. Lower surface roughness values and lower porosities were obtained for the combustion gases ratio of 1:2.5 because of the longer dwelling time of the particles in the hottest zone of the flame.

The thickness of the coatings was not affected by the combustion gases ratio; however, thicker coatings were produced when the spraying distance was larger at a fixed combustion gases ratio.

5 Acknowledgments

The results presented in this paper were possible thanks to the financial support given by *Empresas Públicas de Medellín*, EPM with base in Medellín, Colombia. The authors are also grateful to the Tribology and Surfaces Research Group (GTS) from the Universidad Nacional de Colombia, and the Pyrometallurgy and Materials Research Group (GIPIME) from the Universidad de Antioquia for allowing the use of the equipment used in this work.

6 References

1. Aruna ST, Balaji N, Shedthi J, Grips VKW. Effect of critical plasma spray parameters on the microstructure, microhardness and wear and corrosion resistance of plasma sprayed alumina coatings. *Surface and Coatings Technology*. 2012;208:92-100. DOI: 10.1016/j.surfcoat.2012.08.016

2. Fauchais PL, Heberlein JVR, Boulos M. *Thermal Spray Fundamentals - From Powder to Part*. New York: Springer US; 2014. DOI: 10.1007/978-0-387-68991-3

3. Pawlowski L. Atmospheric Plasma Spraying (APS). In: Pawlowski L. *The Science and the Engineering of Thermal Spray Coatings*. Hoboken: John Wiley and Sons; 2008. p. 74-79.

4. Habib KA, Saura JJ, Ferrer C, Damra MS, Giménez E, Cabedo L. Comparison of flame sprayed Al_2O_3/TiO_2 coatings: Their microstructure, mechanical properties and tribology behavior. *Surface and Coatings Technology*. 2006;201(3-4):1436-1443. DOI: 10.1016/j.surfcoat.2006.02.011

5. Ambiger KD, Kumar A. Anti-Wear Behaviour of Plasmasprayed Alumina & Zirconia Coatings on Aluminium 7075T6. *International Journal of Technical Research and Applications*. 2014;2(4):235-242.

6. Cinca N, Barbosa M, Dosta S, Guilemany JM. Study of Ti deposition onto Al alloy by cold gas spraying. *Surface and Coatings Technology*. 2010;205(4):1096-1102. DOI: 10.1016/j.surfcoat.2010.03.061

7. Di Girolamo G, Serra E. Thermally sprayed nanostructured coatings for anti-wear and TBC applications: State-of-the-art and future perspectives. In: Aliofkhazraei M, ed. *Anti-Abrasive Nanocoatings Current and Future Applications*. Cambridge: Woodhead Publishing; 2015. p. 513-541. DOI: 10.1016/B978-0-85709-211-3.00020-0

8. Jia S, Zou Y, Xu J, Wang J, Yu L. Effect of TiO_2 content on properties of Al_2O_3 thermal barrier coatings by plasma spraying. *Transactions of Nonferrous Metals Society of China*. 2015;25(1):175-183. DOI: 10.1016/S1003-6326(15)63593-2

9. Papitha R, Suresh MB, Chakravarty D, Swarnakar A, Das D, Johnson R. Eutectoid decomposition of aluminum titanate (Al_2TiO_5) ceramics under Spark Plasma (SPS) and Conventional (CRH) thermal treatments. *Ceramics International*. 2014;40(1 Pt A):659-666. DOI: 10.1016/j.ceramint.2013.06.052

10. Sarkar N, Lee KS, Park JG, Mazumder S, Aneziris CG, Kim IJ. Mechanical and thermal properties of highly porous Al_2TiO_5-Mullite ceramics. *Ceramics International*. 2016;42(2 Pt B):3548-3555. DOI: 10.1016/j.ceramint.2015.11.002

11. Li N, Li G, Wang H, Kang J, Dong T, Wang H. Influence of TiO_2 content on the mechanical and tribological properties of Cr_2O_3-based coating. *Materials & Design*. 2015;88:906-914. DOI: 10.1016/j.matdes.2015.09.085

12. Yang K, Rong J, Liu C, Zhao H, Tao S, Ding C. Study on erosion-wear behavior and mechanism of plasma-sprayed alumina-based coatings by a novel slurry injection method. *Tribology International*. 2016;93(Pt A):29-35. DOI: 10.1016/j.triboint.2015.09.007

13. Xu G, Ma Y, Ruan G, Cui H, Zhang Z, Bai B. Preparation of porous Al_2TiO_5 ceramics reinforced by in situ formation of mullite whiskers. *Materials & Design*. 2013;47:57-60. DOI: 10.1016/j.matdes.2012.12.028

14. Lima RS, Marple BR. Enhanced ductility in thermally sprayed titania coating synthesized using a nanostructured feedstock. *Materials Science and Engineering: A*. 2005;395(1-2):269-280. DOI: 10.1016/j.msea.2004.12.039

15. Wang H, Ma J, Li G, Kang J, Xu B. The dependency of microstructure and mechanical properties of nanostructured alumina-titania coatings on critical plasma spraying parameter. *Applied Surface Science*. 2014;314:468-475. DOI: 10.1016/j.apsusc.2014.07.026

16. Ibrahim A, Hamdy AS. Microstructure, Corrosion, and Fatigue Properties of Alumina-Titania Nanostructured Coatings. *Journal of Surface Engineered Materials and Advanced Technology*. 2011;1(3):101-106. DOI: 10.4236/jsemat.2011.13015

17. Yusoff NHN, Ghazali MJ, Isa MC, Daud AR, Muchtar A. Effects of powder size and metallic bonding layer on corrosion behaviour of plasma-sprayed Al_2O_3-13% TiO_2 coated mild steel in fresh tropical seawater. *Ceramics International*. 2013;39(3):2527-2533. DOI: 10.1016/j.ceramint.2012.09.012

18. Gadelmawla ES, Koura MM, Maksoud TMA, Elewa IM, Soliman HH. Roughness parameters. *Journal of Materials Processing Technology*. 2002;123(1):133-145. DOI: 10.1016/S0924-0136(02)00060-2

19. Lutterotti L, Ceccato R, Dal Maschio R, Pagani E. Quantitative Analysis of Silicate Glass in Ceramic Materials by the Rietveld Method. *Materials Science Forum*. 1998;278-281:87-92. DOI: 10.4028/www.scientific.net/MSF.278-281.87

20. Sanches E, Carolino A, dos Santos A, Fernandes E, Trichês D, Mascarenhas P. The use of Le Bail Method to Analyze the Semicrystalline Pattern of a Nanocomposite Based on Polyaniline Emeraldine-Salt Form base and α-Al2O3. Advances in Materials Science And Engineering. 2015 DOI: 10.1155/2015/375312

21. Pawlowski L. *The Science and the Engineering of Thermal Spray Coatings*. Hoboken: John Wiley and Sons; 2008

22. Verbeek ATJ. *Plasma sprayed thermal barrier coatings: production, characterization and testing*. (Thesis). Eindhoven: Eindhoven University of Technology; 1992.

23. Geaman V, Pop MA, Motoc DL, Radomir I. Tribological properties of thermal spray coatings. *European Scientific Journal*. 2013;3(2013):154-159.

24. Rana N, Mahapatra MM, Jayaganthan R, Prakash S. High-Temperature Oxidation and Hot Corrosion Studies on NiCrAlY Coatings Deposited by Flame-Spray Technique. *Journal of Thermal Spray Technology*. 2015;24(5):769-777. DOI: 10.1007/s11666-015-0237-z

25. Rana N, Jayaganthan R, Prakash S. Microstructural Features and Oxidation Behavior of NiCrAlY Coatings Obtained by HVOF Process. *Advanced Materials Research*. 2012;585:507-511. DOI: 10.4028/www.scientific.net/AMR.585.507

26. Yilmaz R, Kurt AO, Demir A, Tatli Z. Effects of TiO_2 on the mechanical properties of the Al_2O_3-TiO_2 plasma sprayed coating. *Journal of the European Ceramic Society*. 2007;27(2-3):1319-1323. DOI: 10.1016/j.jeurceramsoc.2006.04.099

27. Góral A, Żórawski W, Lityńska-Dobrzyńska L. Study of the microstructure of plasma sprayed coatings obtained from Al_2O_3-13TiO_2 nanostructured and conventional powders. *Materials Characterization*. 2014;96(2014):234-240. DOI: 10.1016/j.matchar.2014.08.016

28. Vargas F, Ageorges H, Fournier P, Fauchais P, López ME. Mechanical and tribological performance of Al_2O_3-TiO_2 coatings elaborated by flame and plasma spraying. *Surface and Coatings Technology*. 2010;205(4):1132-1136. DOI: 10.1016/j.surfcoat.2010.07.061

29. Bolelli G, Cannillo V, Lusvarghi L, Manfredini T, Siligardi C, Bartuli C, et al. Plasma-sprayed glass-ceramic coatings on ceramic tiles: Microstructure, chemical resistance and mechanical properties. *Journal of the European Ceramic Society*. 2005;25(11):1835-1853. DOI: 10.1016/j.jeurceramsoc.2004.06.018

30. Palacio CC, Ageorges H, Vargas F, Díaz AF. Effect of the mechanical properties on drilling resistance of Al_2O_3-TiO_2 coatings manufactured by atmospheric plasma spraying. *Surface and Coatings Technology*. 2013;220:144-148. DOI: 10.1016/j.surfcoat.2012.10.075

31. Cadavid Iglesias E, Parra Velásquez C, Vargas Galvis F. Estudio de llamas Oxiacetilénicas Usadas en la Proyección Térmica. *Revista Colombiana de Materiales*. 2016;9:15-26.